Available online at www.sciencedirect.com
ScienceDirect
Trans. Nonferrous Met. Soc. China 21(2011) 1580−1586
Transactions of Nonferrous Metals Society of China
www.tnmsc.cn

Influence of Ga and Bi on electrochemical performance of Al-Zn-Sn sacrificial anodes

HE Jun-guang[1, 2], WEN Jiu-ba[2], LI Xu-dong[1], WANG Guo-wei[2], XU Chun-hua[2]

1. School of Materials Science and Engineering, Lanzhou University of Technology, Lanzhou 730050, China;
2. School of Materials Science and Engineering, Henan University of Science and Technology, Luoyang 471003, China

Received 3 July 2010; accepted 20 December 2010

Abstract: The influence of Ga and Bi on the microstructure and electrochemical performance of Al-7Zn-0.1Sn (mass fraction, %) sacrificial anodes was investigated by means of optical microscopy (OM), scanning electron microscopy/ energy dispersive X-ray analysis (SEM/EDAX) and electrochemical measurements. It was found that the coarse dendrites structure transformed into the equiaxed grains as well as a small amount of dendrite grains after adding Ga and Bi into Al-Zn-Sn alloys. A high current efficiency of 97% and even corrosion morphology were obtained for Al-7Zn-0.1Sn-0.015Ga-0.1Bi alloy. The results indicate that the proper amount of Ga and Bi is effective on improving the microstructure and electrochemical performance of Al-Zn-Sn alloy.
Key words: aluminium; sacrificial anode; electrochemical performance; electrochemical impedance spectroscopy; segregation

1 Introduction

Aluminium is a suitable metal as the sacrificial anodic material for cathode protection of steel components in the seawater due to its high current efficiency, low density and low cost. However, pure aluminium forms a passive film on its surface at an open circuit potential of about −0.8 V(SCE) in seawater [1]. Alloy elements, such as Zn, Hg and In, are used to restrain the formation of passive film and shift the potential towards negative values. Numerous studies have been carried out for exploit Al sacrificial anodes. The current efficiency of Al-Zn-Hg alloy is about 95%, but mercury is toxic, and it has been eliminated from the using. Al-Zn-In alloys have been widely used as the sacrificial anodes in China [2]. Nevertheless, with the production and usage of indium, people have gradually realized that it is harmful to the environment [3]. In order to develop Al sacrificial anode with high-performance and pollution-free, many workers have done a lot of investigation [4−5].

Al-Zn-Sn alloy has a current efficiency of about 70% [6], which is one of the most studied Al sacrificial anodes. Whereas, its efficiency is lower than that of Al-Zn-In alloy. In addition, it requires heat treatment for better performance and higher efficiency. It was reported that bismuth could help in expanding aluminium matrix and thereby increase the solubility of tin in aluminium. GURRAPPA and KARNIK [7] successfully avoided the costly heat treatment process by the controlled addition of a small amount of bismuth to Al-5 Zn-0.25Sn (mass fraction, %) alloy. It is well known that Ga, among others activator elements, could shift the operating potential to more negative value [8]. FLAMINI et al [9] considered that Ga particles at metal/oxide interface could cause local thinning of passive film.

In the present investigation, based on Al-7Zn-0.1Sn (mass fraction, %) alloy, the influence of Ga and Bi on the microstructure and electrochemical performance of Al sacrificial anodes was studied by the microstructure observation and electrochemical measurements. The purpose of this study is to improve the electrochemical performance of Al-Zn-Sn alloy.

2 Experimental

2.1 Material preparation

Raw materials used in experiments include aluminium, zinc, tin, gallium and bismuth (>99.9%, mass

Foundation item: Project (094200510019) supported by Technology Creative Programmer of Henan for Excellent Talents, China; Project (092300410132) supported by the Natural Science Foundation of Henan Province, China
Corresponding author: HE Jun-guang; Tel: +86-379-64231846; Fax: +86-379-64230597; E-mail: he.ellen@163.com
DOI: 10.1016/S1003-6326(11)60900-X

fraction). The nominal compositions of the designed alloys are listed in Table 1. Raw materials were cut, dried, weighed, and melted in a corundum crucible in ZGJL0.01−4C−4 vacuum induction furnace under the argon shield. Then, the fusant at approximately 760 °C was poured into a preheated metal mold of dimensions *d*20 mm×140 mm.

Table 1 Chemical compositions of the experimental alloys

Alloy	*w*(Zn)/%	*w*(Sn)/%	*w*(Bi)/%	*w*(Ga)/%	*w*(Al)/%
I	7	0.1	−	−	Bal.
II	7	0.1	0.1	−	Bal.
III	7	0.1	−	0.015	Bal.
IV	7	0.1	0.1	0.015	Bal.

2.2 Anode current efficiency

The current efficiency tests were carried out with three-electrode system at room temperature with CHI660C electrochemical test system. A saturated calomel electrode (SCE) served as the reference and electrode and mild steel was used as the cathode. The specimen dimensions are *d*16 mm×28 mm, and the surface area of test anode was 14 cm^2. The anode and cathode had surface area in the ratio of 1:60 and were coupled together and immersed in 3.5% NaCl solution at a current density of 1 mA/cm^2 for 10 d. The specimen mass before and after corrosion was measured after cleaning the specimens by standard procedure (GB/T17848—1999) [10]. From the mass loss measured, the current efficiency was calculated.

2.3 Electrochemical measurement

The dimensions for electrochemical measurement were *d*11.3 mm×5 mm. Each specimen was mounted with epoxy resin, leaving an exposed area of 1 cm^2 in contact with the solution. The electrochemical measurements were carried out with three-electrode system by CHI660C electrochemical workstation. A SCE, platinum foil and specimens were used as reference, counter and working electrodes, respectively. Electrochemical impedance spectroscopy (EIS) was recorded in the frequency range from 10 kHz to 0.1 Hz with a perturbation amplitude of 5 mV after immersing the specimens in 3.5% NaCl solution for 4 000 s. Then, the polarizing curve was performed. The scanning range was set from −1.15 to −0.80 V with a constant scan rate of 1 mV/s. The EIS data were fitted with ZsimWin2.0 software.

2.4 Microstructure analysis

The specimens were successively ground to 2000-grit by SiC paper, fine polished with 1.5 μm-diamond paste, etched with 2.5% HNO_3 + 1.5% HCl + 1% HF solution. The microstructures of specimens were characterized using optical microscope (XJ−16B) and scanning electron microscope (SEM, JSM−5610LV) coupled with energy dispersive X-ray (EDX) to identify the phases composition in the alloys. The corrosion morphologies were characterized with digital camera.

3 Results and discussion

3.1 Microstructure

Figure 1 shows the microstructures of as-cast four alloys. The microstructure of alloy I mainly consists of the coarse dendritic structure shown in Fig. 1(a). Whereas, the microstructures of alloys II (Fig. 1(b)), III (Fig. 1(c)) and IV (Fig. 1(d)) were dominated by the equiaxed grains with the size of about 50 μm and a small amount of dendrites, and the dendrite volume fraction in Fig. 1(d) was significantly less than that in Fig. 1(b) or (c). This indicates that the addition of Ga and Bi into Al-Zn-Sn alloy could notably improve the solidification structures, and make the bulky dendritic crystals turn into the small equiaxed crystals.

The SEM micrographs of four alloys are presented in Fig. 2. All alloys mainly consist of *α*(Al) matrix, segregated phases, and grain boundaries with continuous or semi-continuous network. Diffuse boundaries were observed. Parts of the grain boundaries contain some regions with a bright segregated phase and some regions with porosity. The EDX analysis shows that the concentration of Zn and Sn in segregated phase and grain boundaries was higher than that in *α*(Al) matrix for alloys I and III. In the same way, the concentration of Zn, Sn and Bi in segregated phase and grain boundaries was higher than that in *α*(Al) matrix for alloys II and IV. The EDX did not identify the presence of gallium due to its low concentration. It can be seen in Figs.2(b), (c) and (d) that Bi and Ga could reduce the amount of precipitates and the width of diffuse boundaries, so they increase the solubility of Zn in *α*(Al) matrix. Previous studies suggested that Zn in *α*(Al) matrix had an effect mainly on the active behavior of aluminium in chloride solutions [11].

Considering the principle of metal solidification, aluminium with high melting point crystallizes at first. These elements with low melting point, such as Zn, Sn and Bi, are enriched in the liquid ahead of solid-liquid interface during the solidification process, forming the segregation at the grain boundaries. On the other hand, the enrichment of solute atoms leads to low diffusion rate of atoms. Therefore, the number of nuclei formed is increased, and the grain growth is restricted, and the grain is refined. The smaller grains possess a greater area fraction of grain boundaries, which decreases the segregation at the grain boundaries. The fine granular

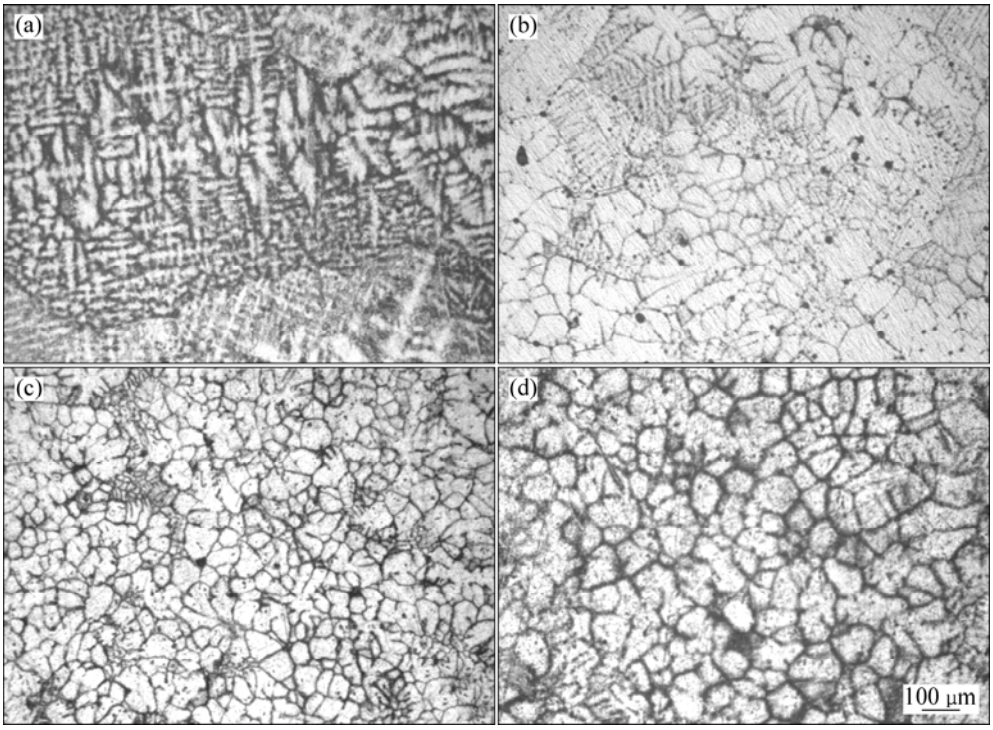

Fig. 1 As-cast microstructures of Al-Zn-Sn series alloys: (a) Alloy I; (b) Alloy II; (c) Alloy III; (d) Alloy IV

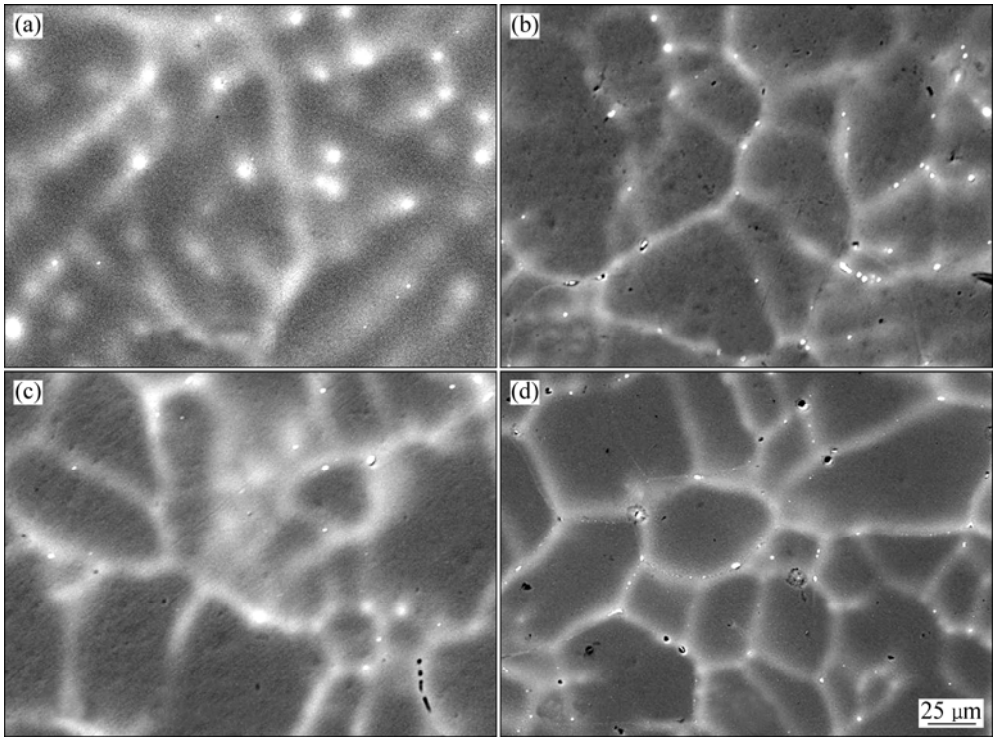

Fig. 2 SEM images of Al-Zn-Sn series alloys: (a) Alloy I; (b) Alloy II; (c) Alloy III; (d) Alloy IV

grains with homogeneous microstructure are gained. The refined equiaxed grains in alloys II, III and IV may be beneficial to improve the electrochemical properties [12].

3.2 Electrochemical performance

The electrochemical properties of alloys I, II, III and IV are listed in Table 2. The current efficiency of alloy I was 76%. A current efficiency of 82% was achieved by adding 0.1% Bi into Al-Zn-Sn alloy. An increase of 20% in current efficiency could be noticed when 0.015% Ga was incorporated into Al-Zn-Sn alloy. The current efficiency increased to 97% after adding

Table 2 Electrochemical performances of four alloys

Alloy	OCP(vs. SCE)/V	Capacity/(A·h·kg^{-1})	Efficiency/%
I	−0.947	2 139	76
II	−1.056	2 303	82
III	−1.091	2 729	96
IV	−1.083	2 753	97

0.015% Ga and 0.1% Bi into Al-Zn-Sn alloy. In addition, the open circuit potential (OCP) of alloy IV tended to be more negative than alloy I. The electrochemical performance was evidently improved through adding Ga or/and Bi into Al-Zn-Sn alloy. The reason may be attributed both to the grain refinement and the low non-coloumbic loss of anodes.

Aluminium sacrificial anode should have the negative and stable close circuit potential (CCP) besides the high current efficiency. The curves of CCP variation versus time for four alloys are shown in Fig. 3. The CCP value of alloy I was about −0.91 V (SCE). The CCP values of alloys II, III and IV shifted to the negative direction, and alloys III and IV had the more negative CCP values and the less fluctuation values compared with alloy II. In addition, the CCP values of four alloys moved to positive value with the increase of immersion time, while the moving values of alloys III and IV were lower than alloys I and II. This indicates that the addition of Ga in Al-Zn-Sn alloy could reduce the degree of anodic polarization during the work process.

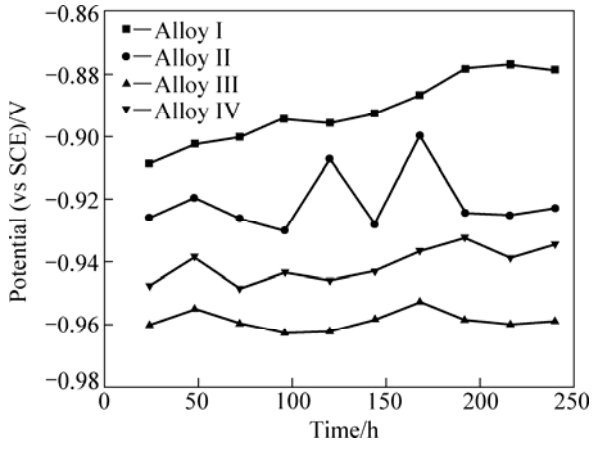

Fig. 3 CCP vs time plots for four alloys in 3.5% NaCl solution

Figure 4 shows the surface features of corroded samples that were cleaned with a solution of 68% HNO_3 after 10 d of immersion. In the case of alloy I or II, the macroattack morphology presented 'metallic sponge' characteristics, and the black corrosion products adhered to the alloy surface during the test process. Serious grain shedding resulted in the poor electrochemical properties. On the contrary, the corrosion products of alloys III and IV fell off easily from the surface of corroded specimens. The surface of alloy III had the big corrosion pits, and the bottom of corrosion pits was coarse, but there was no particles shedding during the test process. Alloy IV dissolved evenly, with only a small amount of undissolved platform could be found, and corrosion areas were flat and smooth. According to the analysis above, the Al-7Zn-0.1Sn-0.015Ga-0.1Bi alloy has the negative and stable CCP values, the uniform corrosion and a high current efficiency.

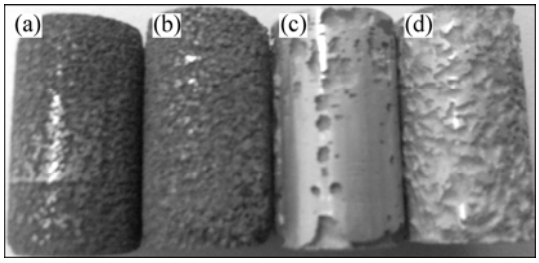

Fig. 4 Surface corrosion features of four alloys after 10 d of immersion: (a) Alloy I; (b) Alloy II; (c) Alloy III; (d) Alloy IV

As stated above, alloy II was activated due to the incorporation of Bi, while the Bi segregation in alloy would cause serious self-corrosion, and the matrix or second phase fell off from the surface alloy, resulting in the 'metallic sponge' feature and the lower current efficiency [13]. Based on the dissolution-precipitation mechanism, the dissolved gallium ions redeposit around the tin inclusion on the surface of Al surface, then Ga accumulates at the grain boundaries along with the Sn inclusion [14], and forms a 'liquid-like' film on the grain boundaries, i.e. Ga-Al amalgam because of the very low melting point of gallium [15], which detaches the oxide film and avoids repassivation. On the other hand, the role of Ga is to bias the surface charge to the direction of activation, and this biased condition facilitates the adsorption of halide anions and makes the alloy active [16]. The particles dropping out from the Al surface are usually less, which leads to a high current efficiency.

3.3 Polarization curves

Figure 5 presents the potentiodynamic polarization curves of four alloys immersed in 3.5% NaCl solution for 4 000 s. The corrosion potential (φ_{corr}) and corrosion current density (J_{corr}) revealed by the potentiodynamic polarization curves of four alloys are listed in Table 3. It is clear that the φ_{corr} values of alloys II, III and IV shifted to less negative values. It was explained by the less segregated particles on the grain boundaries and the uniform distribution of active elements, which resulted from the increase of the solubility of trace elements in α-Al matrix by the incorporation of Ga and Bi. Besides, it could be seen that the polarization curves of alloys I and II showed the formation of pitting corrosion, where a

relatively sharp increase in J_{corr} occurred.

The decrease in non-coulombic loss, the key factor for galvanic efficiency, may be also confirmed by evaluating the corrosion rate of anode. The J_{corr} value is in good agreement with the value of corrosion rate. The J_{corr} value of alloy IV was lower than that of others in Table 3, which implies that the addition of Ga and Bi could decrease the J_{corr} value and bring about low non-coulombic loss.

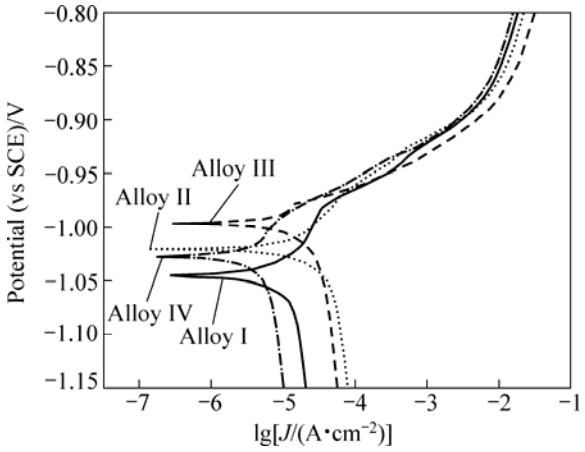

Fig. 5 Potentiodynamic polarization curves of four alloys immersed in 3.5% NaCl solution for 4 000 s

Table 3 φ_{corr} and J_{corr} values of four alloys derived from polarization curves

Alloys	φ_{corr}(vs SCE)/V	J_{corr}/(A·cm^{-2})
I	−1.045	1.522×10^{-5}
II	−1.021	2.588×10^{-5}
III	−0.997	2.497×10^{-5}
IV	−1.028	7.327×10^{-6}

3.4 Electrochemical impedance spectra

Figure 6 displays the Nyquist diagrams of four alloys. A capacitive loop at high frequency and an inductive loop at low frequency could be observed in the diagram of alloys I and II shown in Fig. 6(a). Compared with alloy I, the capacitive loop of alloy II increased significantly, while the inductive loop shrank clearly. On the contrary, there were two capacitive loops, and the inductive loop disappeared for alloys III and IV shown in Fig. 6(b).

It is well known that the capacitive loop at high frequency is attributed to the charge transfer reaction in the electric double layer formed at the interface between the metal surface and the corrosive medium [17], which can be described by charge transfer resistance (R_t) and constant phase element (CPE_1). The R_t is directly associated with the electrochemical corrosion rate. In general, the higher R_t reflects a slower corrosion since the exchange current is directly associated with the

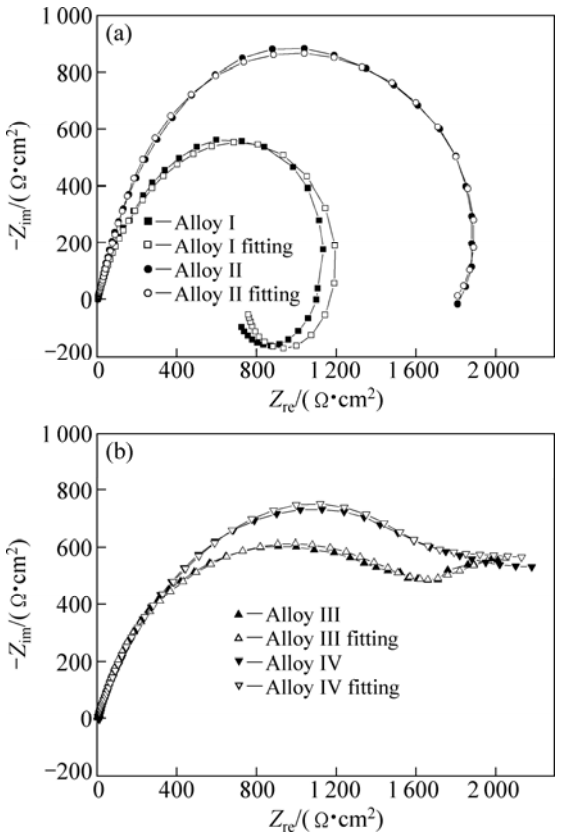

Fig. 6 Nyquist diagrams of four alloys in 3.5% NaCl solution

electrochemical corrosion process. The CPE is used to compensate for the non-homogeneity in the system. It is defined by Y_0 and n ($0\leq n\leq 1$): n=1 corresponds to a capacitor; n=0.5, Warburg impedance; n=0, a resistance; and n=−1, an inductance. The inductive loop at low frequency is contact with the pitting on the alloy surface [18], and R and L are the corresponding parameters for the pitting. The higher R presents to a lower corrosion, which can be ascribed to a good adhesion of adsorbed layer to aluminium surface. The second capacitive loop is generally related to the mass transport in the solid phase [19]. It may be related to the precipitation from Ga ions on the electrode surface, which can be described through CPE_2 and R. R_s represents the solution resistance. Thus, the equivalent circuit of alloys I and II is shown in Fig. 7(a), and that of alloys III and IV is shown in Fig. 7(b).

According to the equivalent circuit mentioned above, the simulation values of the equivalent circuit element obtained by ZsimpWin software are listed in Table 4. The ChiSqr (χ^2) is the precision of the simulated data. It can be seen that χ^2 values were small, indicating that the simulated data are consistent with the experimental ones. Alloy I had the low R_t and high R, implying a fast corrosion and much corrosion production on aluminium surface, corresponding a low current efficiency. Alloy II had the higher R_t and lower R

Table 4 Parameters of equivalent elements in equivalent circuit for four alloys

Alloy	R_s/(Ω·cm^2)	CPE$_1$/(10^{-5} cm^2·Ω^{-1}·s^{-1})	n_1	R_t/(Ω·cm^2)	CPE$_2$/(10^{-3} cm^2·Ω^{-1}·s^{-1})	n_2	R/(Ω·cm^2)	L/(H·cm^2)	$\chi^2/10^{-3}$
I	5.14	7.35	0.79	752.4			977.3	116.4	6.57
II	6.25	1.53	0.92	1 742.0			533.1	47.5	1.75
III	4.63	5.36	0.77	1 758.0	1.54	0.86	1 064.0		2.49
IV	6.32	7.62	0.77	1 791.0	1.62	0.94	1 423.0		1.90

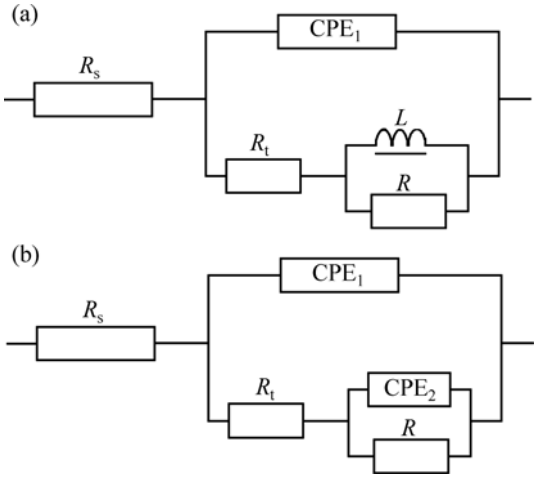

Fig. 7 Equivalent circuits of four alloys in 3.5% NaCl solution: (a) Alloys I and II; (b) Alloys III and IV

compared with alloy I, so the electrochemically properties was improved. Alloys III and IV had the higher R_t without the inductance arc, implying that the pitting caused by self-corrosion and the loss caused by particles falling are smaller, which corresponds to a higher current efficiency.

4 Conclusions

1) The microstructure of Al-Zn-Sn alloy mainly consists of the coarse dendritic structure. After adding Ga or/and Bi into Al-Zn-Sn alloy, the microstructure changes from bulky dendritic crystals to small equiaxed crystals. On the other hand, the addition of Ga or/and Bi into Al-Zn-Sn alloy can evidently improve the distributed uniformity of solidified structure.

2) The current efficiency of Al-Zn-Sn alloys with Ga or/and Bi is markedly higher than that of Al-Zn-Sn alloy. Whereas, Al-Zn-Sn-Bi alloy has a higher self-corrosion, and the dissolved morphology of Al-Zn-Sn-Ga alloy is non-uniform. A high current efficiency and an even corrosion feature can be obtained in the Al-Zn-Sn-Ga-Bi alloy.

3) The potentiodynamic polarization curves show that the corrosion potential of Al-Zn-Sn alloys with Ga or/and Bi shifts to less negative direction compared with Al-Zn-Sn alloy. The corrosion current density of Al-Zn-Sn-Ga-Bi alloy is lower than that of other alloys. The dissolution rate of Al-Zn-Sn alloys containing Ga or/and Bi decreases according to the electrochemical impedance spectra.

References

[1] GONZALEZ C, ALVAREZ O, GENESCA J, JUARE-ISLAS J A. Solidification of chill-cast Al-Zn-Mg alloys to be used as sacrificial anodes [J]. Metall Mater Trans A, 2003, 34(12): 2991−2997.

[2] GB4948—2002. Sacrificial anodes of Al-Zn-In series alloy [S]. Beijing: China Standard Press, 2002. (in Chinese)

[3] WANG Xuan. Indium occupational disease case highlights the policy oversight [J]. Labor Protection, 2008, 55(9): 34−38. (in Chinese)

[4] SHIBLI S M A, JABEERA B, MANU R. Development of high performance aluminium alloy sacrificial anodes reinforced with metal oxides [J]. Mater Lett, 2007, 61(14−15): 3000−3004.

[5] OROZCO R, GENESCA J, JUAREZ-ISLAS J. Effect of Mg content on the performance of Al-Zn-Mg sacrificial anodes [J]. J Mater Eng Perform, 2007, 16(2): 229−235.

[6] KEIR D S, PRYOR M J, SPERRY P R. Galvanic corrosion characteristics of aluminium alloyed with group IV metals [J]. J Electrochem Soc, 1967, 114 (8): 777−782.

[7] GURRAPPA I, KARNIK J A. The effect on tin-activated aluminum-alloy anodes of the addition of bismuth [J]. Corros Prev Control, 1994, 41(5): 117−121.

[8] MANCE A, CEROVIC D, MIHAJLOVIC A. Effect of gallium and phosphorus on the corrosion behaviour of aluminium in sodium chloride solution [J]. J App Electrochem, 1985, 15(3): 415−420.

[9] FLAMINI D O, SAIDMAN S B, BESSONE J B. Aluminium activation produced by gallium [J]. Corros Sci, 2006, 48(6): 1413−1425.

[10] GB17848—1999. Test Methods for electrochemical properties of sacrificial anodes [S]. Beijing: China Standard Press, 1999. (in Chinese)

[11] MUNOZ A G, SAIDMAN S B, BESSONE J B. Corrosion of an Al-Zn-In alloy in chloride media [J]. Corros Sci, 2002, 44(2): 2171−2175.

[12] SINAA H, EMAMYA M, SAREMI M, KEYVANIA A, MAHTA M, CAMPBELL J. The influence of Ti and Zr on electrochemical properties of aluminum sacrificial anodes [J]. Mat Sci Eng A, 2006, 431(1−2): 263−276.

[13] ZHU Cheng-fei, XU Feng, WEI Wu-ji, DING Yi, WANG Ning. Effect of Sb and Sn on performance of aluminum sacrificial anode materials [J]. The Chinese Journal of Nonferrous Metals, 2005, 15(4): 631−636. (in Chinese)

[14] NESTORIDI M, PLETCHER D, WOOD R J K, WANG S C, JONE R L, STOKES K R, WILCOCK I. The study of aluminium anodes for high power density Al/air batteries with brine electrolytes [J]. J Power Sources, 2008, 178(1): 445−455.

[15] TUCK C D S, HUNTER J A, SCAMANS G M. Electrochemical behavior of Al-Ga alloys in alkaline and neutral electrolytes [J]. J Electrochem Soc, 1987, 134(12): 2970−2981.

[16] BRESLIN C B, CARROLL W M. Electrochemical behaviour of aluminium activated by gallium in aqueous electrolytes [J]. Corros Sci, 1992, 33(11): 1735−1739.

[17] MORLIDGE J R, SKELDON P, THOMPSON G E, HABAZAKI H, SHIMIZU K, WOOD G C. Gel formation and the efficiency of anodic film growth on aluminium [J]. Electrochim Acta, 1999, 44(14): 2423−2435.

[18] VENUGOPAL A, RAJA V S. AC impedance study on the activation mechanism of aluminium by indium and zinc in 3.5% NaCl medium [J]. Corros Sci, 1997, 39 (12): 2053−2065.

[19] CABOT P L, GARRIDO J A, PÉREZ E, MOREIRA A H, SUMODJO P T A, PROUN W. EIS study of heat-treated Al-Zn-Mg alloys in the passive and transpassive potential regions [J]. Electrochim Acta, 1995, 40(4): 447−454.

Ga 和 Bi 对 Al-Zn-Sn 牺牲阳极电化学性能的影响

贺俊光[1,2]，文九巴[2]，李旭东[1]，王国伟[2]，徐春花[2]

1. 兰州理工大学 材料科学与工程学院，兰州 730050；
2. 河南科技大学 材料科学与工程学院，洛阳 471003

摘 要：通过光学显微镜(OM)、扫描电镜(SEM)、能谱分析(EDAX)和电化学性能测试等方法，研究了 Ga 和 Bi 对 Al-7Zn-0.1Sn(质量分数，%)牺牲阳极微观组织和电化学性能的影响。Al-Zn-Sn 合金加入 Ga 和 Bi 元素后， 合金组织由粗大枝晶转变为等轴晶，仅剩下少量枝晶。Al-7Zn-0.1Sn-0.015Ga-0.1Bi 合金具有高的电流效率(97%)和均匀的腐蚀形貌，表明添加适量的 Ga 和 Bi 元素能有效改善 Al-Zn-Sn 合金的组织和电化学性能。

关键词：铝；牺牲阳极；电化学性能；电化学阻抗谱；偏析

(Edited by YANG Hua)